

NOVEL SOLUTION TO REYNOLDS EQUATION FOR EXTERNALLY PRESSURISED GAS BEARINGS AS A COMBINATION OF THE SOLUTIONS OF TWO INITIAL VALUE PROBLEMS

Adrian Cazan¹

Keywords:

Externally pressurized gas journal bearing; Recess volume; Bearing coefficients; Whirl ratio; Boundary differential equation; Initial value problem.

ABSTRACT

This paper presents a novel method which generates the solution of Reynolds boundary value differential equation as a combination of the solutions of two initial value problems (IVP). By using the linearized PH theory, the results for the concentric Externally Pressurized Gas Bearing (EPB) were used to solve the case of a steady state eccentric EPB. The method was also used to investigate the influence of the feeding recess volume on the cylindrical whirl threshold ratio and bearing coefficients as well as for the calculation of the transition point between unchoked to choked flow. The results have engineering significance as the EPB coefficients are shown to vary considerably due to the interaction between the recess volumes and the journal vibration. Also, the transition from choked to unchoked flow changes the gas bearing dimensionless flow and, as a result, the inlet pressure values. The Mathematica program used to implement the method has the advantage that it does not require grid spacing, or an estimated number of intermediate points. It employs standard Mathematica build-in functions, therefore easier to design and use for engineering applications. The calculated results and graphs are in fair agreement with available foundational experimental and theoretical published work.



© 2020 Published by Faculty of Engineering

1. INTRODUCTION

In order to construct a solution to the boundary value problem describing the gas bearings a general solution to the associated differential equation is required. In most cases, the solution is found by using numerical methods. For the specific case of gas bearing's Reynolds equation, a Robin boundary condition is derived. Over the years different numerical methods were used for finding a solution to this problem.

The application of finite difference methods (Pink, 1976, Pink, 1981) was initially employed for the analysis of the theoretical performance of hybrid bearings. The results demonstrated the variation of the aerodynamic component of lift versus a varying speed, L/D ratio and supply pressure.

Another numerical approach was the use of trapezoidal rule and the pressure perturbation method for the analysis of the effect of journal rotation and vibration on the performance of externally pressurized gas journal

¹ Corresponding author: Adrian Cazan
Email: adrian.cazan@aurak.ac.ae

bearings (Lund, 1964). The row of the feeding holes was approximated as a line source. The threshold of instability was numerically solved as a function of supply pressure, feeding parameter and eccentricity ratio. The solution was found as a finite series in which the initial terms were generated from the initial conditions.

Alternatively, Runge- Kutta method was used for solving Reynolds equation for an EPB with one row of feeding holes [(Fleming 1970) and two rows of feeding holes (Uneeb and Gohar, 1997).

An approximated solution of the load capacity of an EPB was found by solving a linearized Reynolds equation by finite difference method (FEM) (Zhang, Zhu and Yang, 2008).

A different approach for the calculation of the EPB pressure distribution was the use of Newton`s method and successive relaxation methods for faster convergence (Liu, Zhang and Xu, 2008).

More recently a more accurate second order finite difference method in conjunction with an iterative procedure for solving the gas bearing perturbed Reynolds was published (Wang, Xu, Wang, Zhang, Yang and Peng, 2017).

In this paper the transformation of boundary value problems into initial value problems mathematical method (Ascher and Russell, 1981; Klamkin, 1970) is extended to complex functions. The method was implemented into a computer program by using Mathematica programming language. The program was designed, tested and validated as a practical engineering tool for an accurate assessment of the parameters and performance of Externally Pressurized Gas Journal Bearing working in a vertical and steady state position.

2. ANALISYS

A subsequent analysis and comparison of different externally pressurized bearings` performance and to generate design criteria and charts of general validity requires the definition of specific dimensionless groups. These groups are derived from the basic equations describing the pressure distribution in the gas bearing and from Reynolds equation expressed in a polar system of coordinates. Figure 1 shows a typical aerostatic journal bearing with one central row of feeding holes.

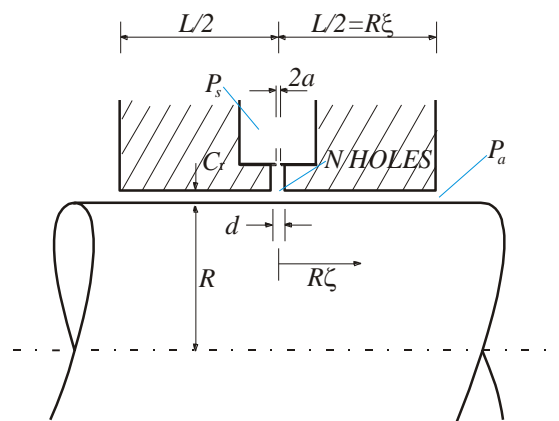


Figure 1. E.P.B. Section

The system analysed in this paper is composed by two identical EPB`s constraining a vertical axis rotor (or only one whose eccentricity ratio is negligible). Initially, the rotor centre of mass is equidistant between the bearings and coincident with its geometric centre. The bearings are externally pressurized, each with one central row of feedholes. When the rotor spin axis suffers a small radial perturbation, only cylindrical whirl is assumed.

The tangential component of the aerodynamic damping force acts on the orbiting rotor centre and according to the sign of this force, the rotor centre will either spiral inwards back towards its equilibrium position (for a negative sign) or will spiral outwards (for a positive sign). At the stability limit, when the tangential damping force is zero, the rotor centre will start to move on a circular orbit. For an externally pressurized gas bearing, the following dimensionless groups are defined:

$$\phi = \tau = \Omega t, \theta = \frac{x}{R}, \zeta = \frac{z}{R}, \tau = \Omega * t, H = \frac{h}{c_r}, \quad (1)$$

$$P = \frac{p}{p_a}, \Lambda = \frac{6\mu\omega}{p_a} \left(\frac{R}{c_r}\right)^2, \sigma = \frac{12\mu\Omega}{p_a} \left(\frac{R}{c_r}\right)^2$$

Using the above defined dimensionless groups Reynolds equation in a fixed system of coordinates is derived as:

$$\frac{\partial}{\partial \theta} \left(H^3 \frac{\partial P^2}{\partial \theta} \right) + \frac{\partial}{\partial \zeta} \left(H^3 \frac{\partial P^2}{\partial \zeta} \right) = 2 \left[\Lambda \frac{\partial (PH)}{\partial \theta} + \sigma \frac{\partial (PH)}{\partial \tau} \right] \quad (2)$$

As shown in Figure 2 a rotating system of coordinates is introduced by the substitution:

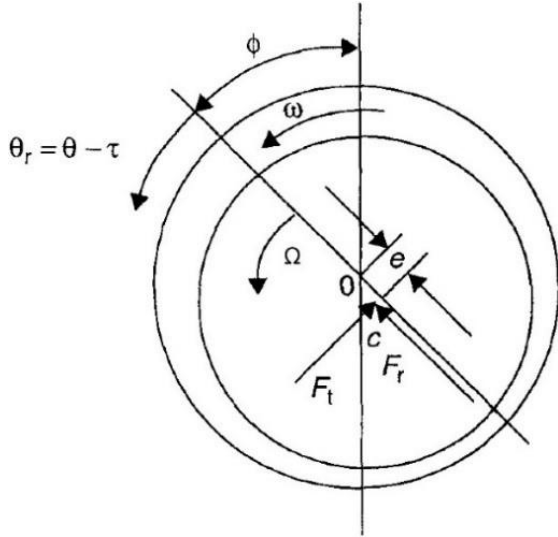


Figure 2. Rotating system of coordinates

The dimensionless film thickness, H , is expressed as:

$$H = 1 + \varepsilon \cos(\theta_r) \quad (4)$$

Substituting equations (3) and (4) into equation (2) it results:

$$\frac{\partial}{\partial \theta_r} \left(H^3 \frac{\partial P^2}{\partial \theta_r} \right) + \left(H^3 \frac{\partial P^2}{\partial \zeta^2} \right) = \quad (5)$$

$$2(\Lambda - \sigma) * \left[H \frac{\partial P}{\partial \theta_r} - P \varepsilon \sin(\theta_r) \right]$$

2.1 Boundary Conditions for Single Orifice Entry

At the midplane of the bearing, the axial mass flow per unit length of circumference must equal one-half the mass flow through a unit length of the feeding line added to the rate of change of gas in the feeding pocket with time. Consider the mass flow G_i out of the bearing at one side as shown in Figure 3:

$$G_i = - \frac{\rho h^3}{12\mu} \frac{dp}{dz} \quad (6)$$

The density of the gas, ρ , can be related to the film dimensionless pressure by using the gas state equation such as:

$$\rho = \frac{P_a}{R_S T_S} P \quad (7)$$

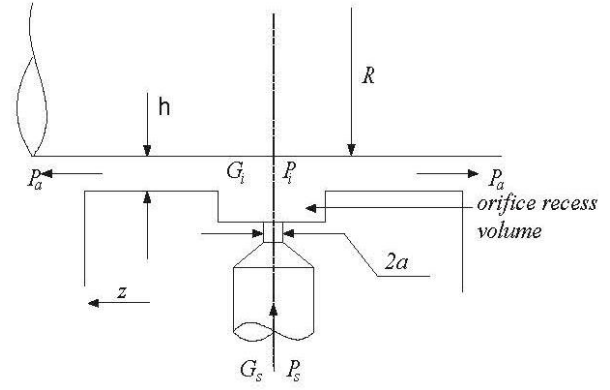


Figure 3. Gas flow in an EPB with a single row of feeding holes with recess volume

The boundary condition relates the flow through a feeding hole with the out flow through a strip line of the bearing. Although in practice, there are a finite number of feedholes, in order to make the problem tractable it was assumed that the row can be represented by a line source as it enters the film (Powell, 1963). A common parameter of these flows is the inlet pressure P_i (the dimensionless pressure immediately under the hole). Substituting equation (11) and the dimensionless bearing groups defined by equations (2), the mass flow G_i is calculated as:

$$G_i = - \frac{c_r^3 H^3}{R_S T_S} \frac{PdP}{d\zeta} \frac{(p_a)^2}{R} \quad (8)$$

The flow into the orifice (and out of one side) is:

$$G_s = \frac{\pi a^2 p_s}{\sqrt{R_S T_S}} \frac{1}{\sqrt{1 + \delta}} \frac{N}{4\pi R} m \quad (9)$$

where $\underline{\delta} = \frac{\delta}{H}$, $\delta = \frac{a^2}{c_r d}$ and m is the dimensionless mass flow. G_i and G_s are linked by:

$$G_i = G_s - \frac{\partial(\rho_i V_i)}{\partial t} \frac{N}{4\pi R} \quad (10)$$

where V_i is the orifice recess volume (refer to Figure 3). The partial derivative expresses the rate of change of gas in pocket with time. By using equation (6) and the system of rotating coordinates in which it is assumed that the journal is rotating with a constant angular whirl speed Ω , the equation (10) is reduced to:

The term $\frac{\partial P_i}{\partial \theta_r} \frac{N}{4\pi R} \frac{p_a V_i \Omega}{R_S T_S}$ in the equation (11) shows

that at a fixed pocket in the bearing wall, the journal surface moves away and towards it as it whirls with a constant speed, Ω .

The dimensionless mass flow m for a perturbed position of the journal is related to the dimensionless mass flow in the initial concentric position as follows:

$$m = m_0 + \left(\frac{\partial m}{\partial P_i}\right)_{\varepsilon=0}(\Delta P_i) \quad (12)$$

In the equation (11) the sub index “ i ” for P refers to the inlet film perturbed pressure.

The dimensionless inlet pressure P_i can be written as a first order perturbation:

$$P_i(\theta_r, \zeta) \cong P_{0i} + \varepsilon P_{1i}(\theta_r, \zeta) \quad (13)$$

The inlet pressure variation is:

$$\Delta P_i = P_i - P_{0i} = \varepsilon P_{1i} \quad (14)$$

The dimensionless mass flow is also calculated from the theoretical equation for one-dimensional, steady, isentropic flow of an ideal, gas through a nozzle, assuming the gas accelerates from stagnation conditions:

$$m = v \sqrt{\frac{2k}{k-1} \left(\frac{P_i}{P_s}\right)^{\frac{1}{k}} \sqrt{\left[1 - \left(\frac{P_i}{P_s}\right)^{\frac{k-1}{k}}\right]}} \quad (15)$$

$$\text{for } \frac{P_i}{P_s} > \left(\frac{2}{k+1}\right)^{\frac{k}{k-1}}$$

$$m = v \sqrt{\frac{2k}{k+1} \left(\frac{2}{k+1}\right)^{\frac{1}{k-1}}} \quad (16)$$

$$\text{for } \frac{P_i}{P_s} \leq \left(\frac{2}{k+1}\right)^{\frac{k}{k-1}}$$

In the above equations v is orifice vena contracta coefficient (Figure 4) and k is the adiabatic gas exponent.

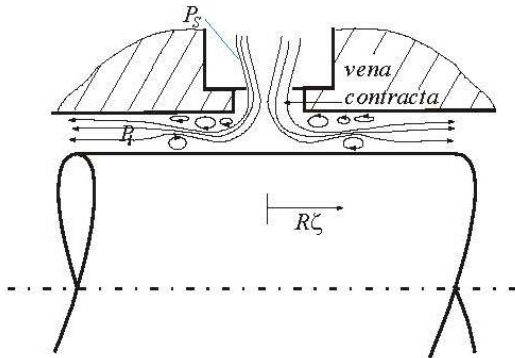


Figure 4. Gas flow profile downstream of the feeding hole

The set of formulae (15) and (16) presents two formulae for the dimensionless mass flow, m , according to the pressure ratio value, P_i/P_s . The threshold value of the pressure ratio has a physical meaning: it shows the transition from the subsonic speed to sonic speed (at the minimum area of flow). The subsonic speed is associated with unchoked flow, while sonic speed is associated with choked flow. Equation (16) shows that the dimensionless choked mass flow has a constant value, independent of the pressure ratio. Parameter k is the adiabatic gas exponent in the above formulae. Particularly for orifices, the flow continues to contract upon leaving the orifice. The parameter v is named “discharge coefficient” or “vena contracta coefficient” and takes into account the contraction of the gas flow. The value of the discharge coefficient is given by the ratio of the actual flow rate to the theoretical flow rate. From equations (8) and (11) results:

$$-\frac{c_r^3 H^3}{R_S T_S} \frac{PdP}{12\mu} \frac{p_a}{d\zeta} \frac{p_a}{R} = G_s + \frac{\partial P_i}{\partial \theta_r} \frac{N}{4\pi R} \frac{p_a V_i \Omega}{R_S T_S} \quad (17)$$

By substituting equations (8), (9), (12), (14) into equation (17) and sorting the resulting terms according to the powers of the perturbation parameter ε (dimensionless eccentricity) a system of two equations is identified. The first equation is:

$$\frac{\partial(P_0^2)}{\partial \zeta} = -q \quad (18)$$

Equation (18) shows the boundary condition at the bearing feeding mid-plane for the bearing with the journal in the concentric position.

The second equation is:

$$\frac{\partial P_0 P_1}{\partial \zeta} = q \frac{(1.5 + \delta^2)}{(1 + \delta^2)} \text{Cos}(\theta_r) - \sigma \psi_1 \left(\frac{\delta P_0 P_1}{\delta \theta_r}\right) + \psi_0 (P_0 P_1) \quad (19)$$

The rest of the pressure boundary equations are found in the following way: At each end of the bearing ($\zeta = \xi$) the pressure is atmospheric:

$$P_0(\xi) = 1 \quad (20)$$

$$P_1(\xi) = 0$$

The pressure is symmetric about the midplane ($\zeta = 0$) therefore:

$$\left(\frac{\partial P_0}{\partial \zeta} = \frac{\partial P_1}{\partial \zeta}\right)_{\zeta=0} = 0 \quad (21)$$

Equations (18), (19), (20), (21) express the E.P.B. boundary conditions. During the simplification process of equation (20) a number of groups are identified and introduced in the boundary equations such as:

$$\psi_0 = -\frac{\lambda_t}{P_{0i}} \frac{\partial m}{\partial \left(\frac{P_i}{P_s}\right)}_{\varepsilon=0} \quad (22)$$

$$\psi_1 = \frac{NV_i}{\pi(2R)^2 c_r P_{0i}} = \frac{vL}{P_{oi} 2R} \quad (23)$$

$$\lambda_t = \frac{6\mu Na^2 \sqrt{\eta R_s T_s}}{p_a c_r^3 \sqrt{1 + \delta^2}} \quad (24)$$

$$P_s = \frac{P_s}{P_a} \quad (25)$$

$$q = \lambda_t P_s m_0 \quad (26)$$

Equation (26) determines q . The line source concept can lead to considerable errors in the flow rate estimate through the bearing clearance, particularly when the number of feeding holes is small. Therefore, a formula for a correction factor was derived based on the method of sources and sinks (Lund, 1967, Mori and Mori, 1971). The flow is defined in terms of a potential or driving force, much like one defines an electric field using voltages. According to the assumptions of zero eccentricity and parallel plate flow, the externally pressurized bearing is opened out to represent a flat two-dimensional flow, where each orifice is represented by a point source.

Based on the above-mentioned assumptions Lund (1967) estimated the correction coefficient, λ , as:

$$\lambda = \frac{1}{N\zeta} \sum_{n=-\infty}^{n=\infty} (-1)^n * \quad (27)$$

$$Ln\left\{ \frac{\text{Cosh}[N\zeta(2n+1)] - 1}{\text{Cosh}(2Nn\zeta) - \cos\left(\frac{Nd}{D}\right)} \right\}$$

In the above equation $\zeta = \frac{L}{2R}$, n is the summation index and N is the number of feeding holes. Therefore, the corrected formula for q is:

$$q = \lambda \lambda_t P_s m_0 \left(\frac{P_0(\zeta)}{P_s}\right) \quad (28)$$

Figure 5 illustrates the pressure distribution contour plots for an externally pressurized gas bearing with one row of feeding holes.

The constant pressure contour plots calculations were performed using a program written in Mathematica language for an E.P.B. with the following characteristics:

$P_a = 10^5 \text{N/m}^2$; $\xi = 0.75$; $P_s = 4.8$; $R = 0.01585 \text{m}$;
 $N = 8$ feeding holes; $d = 0.0011 \text{m}$; $L/D = 1$;
 $c_r = 3.6 * 10^{-5} \text{m}$; $a = 0.00055 \text{m}$;

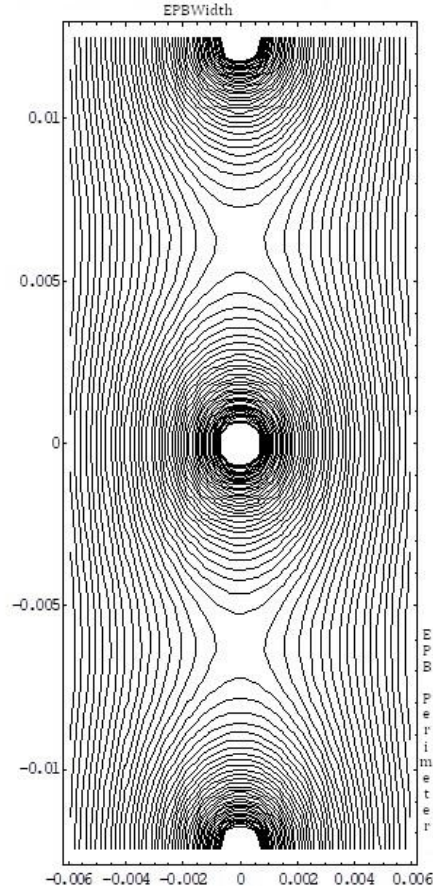


Figure 5. Contours of constant pressure distribution

2.2 First order perturbation method applied E.P.B. Reynolds Equation

A first order perturbation around the journal concentric position can be assumed by using equation (4) and a first order pressure perturbation, (Lund, 1964, Lund, 1967):

$$P(\theta_r, \zeta) \cong P_0 + \varepsilon P_1(\theta_r, \zeta) \quad (29)$$

Substituting equations (29) and equations (4) into equation (5) and considering the resultant expression as an identity in ε in which the powers of ε greater than 1

are neglected, then the following two equations are found:

$$\frac{\partial^2 P_0^2}{\partial \zeta^2} = 0 \quad (30)$$

$$\frac{\partial^2 P_0 P_1}{\partial \theta_r^2} + \frac{\partial^2 P_0 P_1}{\partial \zeta^2} - (\Lambda - \sigma) \left(\frac{1}{P_0} \frac{\partial^2 P_0 P_1}{\partial \theta_r^2} - P_0 \sin(\theta_r) \right) = 0 \quad (31)$$

P_0 is the pressure around a concentric journal therefore it does not depend on θ_r and can be integrated as:

$$P_0^2 = 1 + q(\zeta - \zeta) \quad (32)$$

where q is a boundary condition determined from flow conditions expressed by equation (28). Equation (31) can be further transformed by assuming:

The resulting equation is:

$$G''(\zeta) - G(\zeta) + i(\Lambda - \sigma) \left[\frac{G(\zeta)}{P_0} + P_0 \right] = 0 \quad (34)$$

The associated boundary conditions (18) and (19) become for the function $G(\zeta)$:

$$\text{for } \zeta = \xi \quad G(\xi) = 0 \quad (35)$$

$$\text{And for } \zeta = 0 \quad (36)$$

$$G'(0) = q \frac{(1.5 + \delta^2)}{(1 + \delta^2)} + G(0)(\sigma\psi_1 + \psi_0)$$

The solution of equation (34) allows for the calculation of bearing forces by integrating of the pressure:

$$F_r = - \int_{-\frac{L}{2}}^{\frac{L}{2}} d\zeta \int_0^{2\pi} p_a P(-\cos(\theta)) R d\theta \quad (37)$$

$$F_t = - \int_{-\frac{L}{2}}^{\frac{L}{2}} d\zeta \int_0^{2\pi} p_a P \sin(\theta) R d\theta \quad (38)$$

The dimensionless radial and tangential forces are defined as:

$$f_r = \frac{\Pi}{2\zeta} \left(-\text{Re} \int_0^\zeta \frac{G(\zeta)}{P_0} d\zeta \right) = \frac{F_r}{\varepsilon P_a L D} \quad (39)$$

$$f_t = \frac{\Pi}{2\zeta} \left(\text{Im} \int_0^\zeta \frac{G(\zeta)}{P_0} d\zeta \right) = \frac{F_t}{\varepsilon P_a L D} \quad (40)$$

The resultant load and respectively the attitude angle are:

$$W = \sqrt{F_r^2 + F_t^2} \quad (41)$$

$$\phi = \tan^{-1} \left(\frac{F_t}{F_r} \right) = \tan^{-1} \left(\frac{f_t}{f_r} \right) \quad (42)$$

It can be noticed that even if the bearing is unloaded and vertical, an altitude angle, ϕ_0 , can still be defined as:

$$\phi_0 = \tan^{-1} \left(\frac{f_{t0}}{f_{r0}} \right) = \tan^{-1} \left(\frac{F_{t0}}{F_{r0}} \right) \quad (43)$$

Where the subscript “ o ” indicates the steady state for the vertical EPB ($\sigma=0$). For the dynamic equations the radial and tangential forces are assumed to have the following expressions (Mori and Mori, 1973; Cazan, Ghohar and Safa, 2002):

$$F_r = K |\bar{e}| \quad (44)$$

$$F_t = C |\bar{e}| \quad (45)$$

At marginal stability $\dot{\theta}_r$, is replaced by Ω . In case of steady state $\Omega=0$. The following equations can be used for the physical dynamic stiffness and damping coefficients K , C (Unee and Gohar, 1997):

$$K = \lim_{|\bar{e}| \rightarrow 0} \left(\frac{F_r}{|\bar{e}|} \right) \quad (46)$$

$$C = \lim_{(|\bar{e}|, \omega, \Omega) \rightarrow 0} \left(\frac{F_t}{|\bar{e}|} \right) \quad (47)$$

The normalized stiffness and the damping film coefficients can be calculated assuming that the radial component is due to stiffness and the quadrature component is the damping force due to the squeeze action between the journal and the bearing surfaces. The defining equations (Mori and Mori, 1971) for the normalized coefficients are:

$$k_n = \frac{K}{\psi P_a L \left(\frac{D}{c_r} \right)} \quad (48)$$

$$c_n = \frac{Cc_r}{\psi \left(\frac{12\mu}{p_a} \left(\frac{D}{2c_r} \right)^2 LDp_a \right)} \quad (49)$$

The variation in percentages of the normalized stiffness and damping coefficients are calculated as follows:

$$(\Delta k_n)\% = \frac{k_{n0} - k_{nV}}{k_{n0}} \times 100 \quad (50)$$

$$(\Delta c_n)\% = \frac{c_{n0} - c_{nV}}{c_{n0}} \times 100 \quad (51)$$

Where k_{n0} , c_{n0} are the normalized stiffness and damping coefficients for null recess volume and k_{nV} and c_{nV} are the normalized stiffness and damping coefficients for non-zero recess volume. In the equations (48) and (49) a correction factor, ψ , was introduced in order to take into account the discreteness of the feeding sources as opposed to the feeding line concept used in the mathematical model of the gas bearing. The correction factor, ψ , is used for correcting the bearing coefficients

(Mori and Mori, 1971; Mori and Mori, 1973) while λ (Lund, 1967) is applied to the massless bearing flow, q , as shown by equation (28). The relation between λ and ψ is that $\lambda=1/\psi$.

2.3 Linearized PH theory for steady state finite eccentricity

The method presented in the previous section can be employed for solving the horizontal loaded E.P.B. working in an eccentric steady state position as shown in Figure 6. A first approximation to the finite eccentricity effects are found based on the linearized PH method of analysis for a plain cylindrical gas bearing (Ausman, 1961; Ghosh, Majumdar, Sarangi, 2014). For the steady state case the dimensionless pressure P can be approximated as:

$$P = \frac{P_0 + \varepsilon_0(P_1 + P_0 \cos(\theta))}{1 + \varepsilon_0 \cos(\theta)} = P_0 + \frac{\varepsilon_0 P_1}{1 + \varepsilon_0 \cos(\theta)} \quad (52)$$

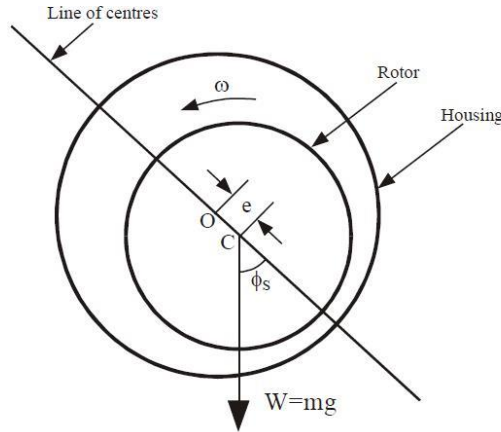


Figure 6. E.P.B. in steady state position

P_0 and P_1 are the vertical E.P.B. calculated pressures and ε_0 is the dimensionless eccentricity for the steady state case. The E.P.B. forces for the steady state eccentric position are related to the previously calculated forces for the vertical EPB by the formulas:

$$F_{RS} = \frac{2}{\sqrt{1-\varepsilon_0^2} (1 + \sqrt{1-\varepsilon_0^2})} F_{r0} \quad (53)$$

$$F_{TS} = \frac{2}{1 + \sqrt{1-\varepsilon_0^2}} F_{t0} \quad (54)$$

Where ε_0 is the steady state eccentricity. F_{r0} and F_{t0} are forces acting on the concentric EPB when $\sigma=0$. The dimensionless radial and tangential forces can be calculated as:

$$f_{RS} = \frac{2\varepsilon_0}{\sqrt{1-\varepsilon_0^2} (1 + \sqrt{1-\varepsilon_0^2})} f_{r0} \quad (55)$$

$$f_{TS} = \frac{2\varepsilon_0}{1 + \sqrt{1-\varepsilon_0^2}} f_{t0} \quad (56)$$

The static equilibrium equations are:

$$\frac{W}{p_a LD} = f_{RS} \cos(\phi_s) + f_{TS} \sin(\phi_s) \quad (57)$$

$$0 = -f_{RS} \sin(\phi_s) + f_{TS} \cos(\phi_s) \quad (58)$$

3. PROPOSED SOLUTION

Equation (34) is a differential equation subject to Robin boundary condition, also known as third type boundary conditions. These conditions are displayed expressed by the equations (35) and (36). The general solution of equation (34) can be expressed as a combination of the solutions two initial value problems (IVP):

$$G(\zeta) = G_1(\zeta) + AG_2(\zeta) \quad (59)$$

By substituting equation (69) into equation (34), $G_1(\zeta)$ and $G_2(\zeta)$ are identified as solutions of the following differential equations with the associated initial conditions:

$$G_1''(\zeta) - G_1(\zeta) + i(\Lambda - \sigma) * \quad (60)$$

$$\left[\frac{G_1(\zeta)}{P_0} + P_0 \right] = 0 \quad (61)$$

$$G_1(0) = 1, \quad G_1'(0) = q \frac{(1.5 + \delta^2)}{(1 + \delta^2)}$$

$$G_2''(\zeta) - G_2(\zeta) + i(\Lambda - \sigma) \left[\frac{G_2(\zeta)}{P_0} \right] = 0 \quad (62)$$

$$G_2(0) = 1, \quad G_2'(0) = \sigma\psi_1 + \psi_0 \quad (63)$$

The boundary condition at $\zeta=0$ is satisfied automatically. The value of A is determined from the boundary condition at $\zeta=\xi$ as:

$$A = - \frac{G_1'(\xi) + G_1(\xi)}{G_2'(\xi) + G_2(\xi)} \quad (64)$$

With the condition:

$$G_2'(\xi) + G_2(\xi) \neq 0 \quad (65)$$

Therefore, the solution of equation (34) can be written as:

$$G(\zeta) = G_1(\zeta) - \frac{G_1'(\xi) + G_1(\xi)}{G_2'(\xi) + G_2(\xi)} G_2(\zeta) \quad (66)$$

By substituting dimensionless mass flow q from equation (28) into equation (32) it follows:

$$P_0^2(\xi) - 1 = \lambda \lambda_t P_s m_0 \left[\frac{P_0(\xi)}{P_s} \right] \quad (67)$$

The value of $P_0(\xi)$ was numerically calculated from equation (67) using Mathematica software. As equation (67) does not have a closed form solution, the Mathematica symbol **FindRoot** was used within the procedure for calculating $P_0(\xi)$. The functions $G_1(\zeta)$ and

$G_2(\zeta)$ were determined as interpolation functions by using as part of the procedure the Mathematica symbol **NDSolve** which can be applied for solving differential equations involving complex numbers. Another original feature of the program is the check of gas flow conditions. According to the value of the ratio between the pressure at film inlet and the supply pressure, the gas flow can be either choked or not, according to the system of equations (15) and (16). An initial dimensionless mass flow value, q_a , is required for the flow check iterative procedure. The "initial guess" for initiating the procedure was calculated using the following formula [3]:

$$q_a = \frac{1}{2} \xi \lambda_t^2 \left\{ -1 + \left[1 + 4 \frac{V^2 - 1}{\xi^2 \lambda_t^2} \right]^{\frac{1}{2}} \right\} \quad (68)$$

For the steady state eccentric E.P.B. the substitution of the equations (55) and (56) into the equations (57) and (58) generates a new system of equations containing as unknowns the steady state eccentricity ε_0 and the steady state attitude angle ϕ_s . The numerical solution of this system of equations was calculated using a numerical procedure involving the Mathematica symbol **FindRoot**.

4. RESULTS

The results presented in this section show the main characteristics of a vertical (or negligible eccentricity) and for the finite steady state eccentricity E.P.B. The E.P.B. and its gas supply have the following physical characteristics:

$p_a = 10^5 \text{ N/m}^2$, $R = 0.02 \text{ m}$, $N = 8$ feeding holes,
 $d = 0.001 \text{ m}$, $a = 0.0002 \text{ m}$,
 T_S (temperature) = 305 K°,
 η (adiabatic efficiency) = 0.6,
 k (adiabatic index) = 1.4,
 ν (vena contracta coefficient) = 0.87,
 R_S (gas constant) = 29.27 kgfm/kg K°,
 $\mu = 1.9 * 10^{-5} \text{ Ns/m}^2$

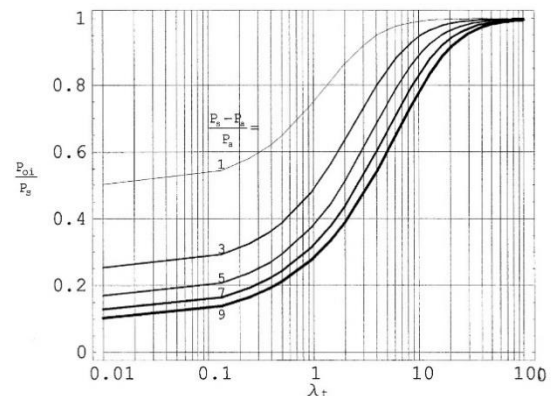


Figure 7. Concentric pressure ratio P_{0i} versus the feeding parameter (λ_t)

Figure 7 presents the variation of the concentric pressure ratio P_{0i} versus the feeding parameter (λ_i) for an EPB with $L/D=1$. A family of plots was generated for different values of the dimensionless supply pressure. P_{0i} has an asymptotic relationship with λ_i . It can be seen that the increase in the feeding parameter results in P_{0i} approaching unity (i.e. equal to the supply pressure). For low values of the feeding parameter λ_i , the inlet pressure gradient is almost zero (for $\lambda_i < 0.01$). This may be caused by the change in the flow conditions respectively the transition from “Unchoked Flow” to “Choked Flow”.

In particular, as $\lambda_i \rightarrow \infty$ the clearance $\rightarrow 0$. Therefore, there is no flow, making $P_{0i} \rightarrow 1$ (inlet pressure equals the supply pressure).

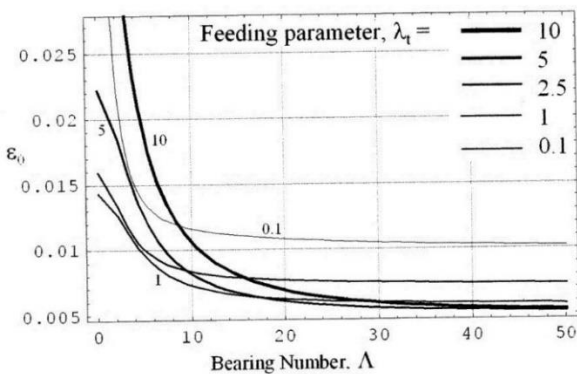


Figure 8. Eccentricity versus bearing number, A , with λ_i as parameter ($L/D=1$, $P_s=3$, $m_1=0.5Kg$)

Figure 8 shows the eccentricity versus bearing number, A . The dimensionless length has the value of 1. The eccentricity decreases with the increase in bearing number. For a bearing number higher than 20 the eccentricity remains almost constant. The increase in the feeding parameter has the result of decreasing the eccentricity. The feeding parameter is directly related to the aerostatic forces generated within the gas film. Therefore, for higher values of the feeding parameter ($\lambda_i > 1$) the eccentricity curves will converge due to the predominant hydrostatic effect.

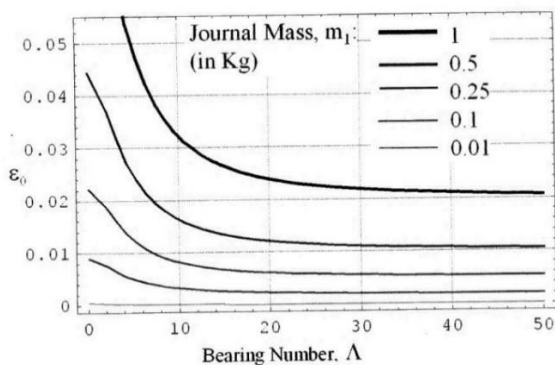


Figure 9. Eccentric Steady State E.P.B. Dimensionless eccentricity versus bearing number with mass, m_1 , as parameter ($L/D = 1$, $P_s=3$, $\lambda_i=5$)

Figure 9 shows the variation of the eccentricity versus the bearing number A . The dimensionless supply pressure has the value 3, and the dimensionless length has the value of 1. The graphs present a hyperbolic trend except the curve representing the eccentricity associated with mass equal to 0.01. This curve represents an unloaded bearing and it was produced in order to test the software in a limit case. The expected value was a constant eccentricity of value 0, which the software produced accurately. The increase in the mass has the effect of a proportional increase in the eccentricity. The eccentricity tends to constant values at high speed as the aerostatic component loses its influence.

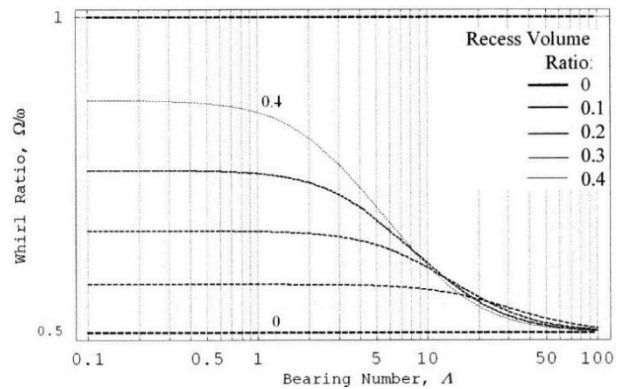


Figure 10. Whirl Ratio (Ω/ω) versus Bearing Number (A) at marginal stability ($\lambda_i=1$, $P_s=2$, $L/D=1$)

Figure 10 presents the whirl ratio versus the bearing number at marginal stability. The feeding parameter λ_i has the value 1, the dimensionless supply pressure is 2, the dimensionless length is 1 and the recess volume has the values 0, 0.1, 0.2, 0.3, 0.4. It can be seen that the value of the whirl ratio is higher than 0.5 for relatively small bearing numbers values and for recess volume > 0 . The value of the whirl ratio tends asymptotically towards 0.5, when the bearing number increases.

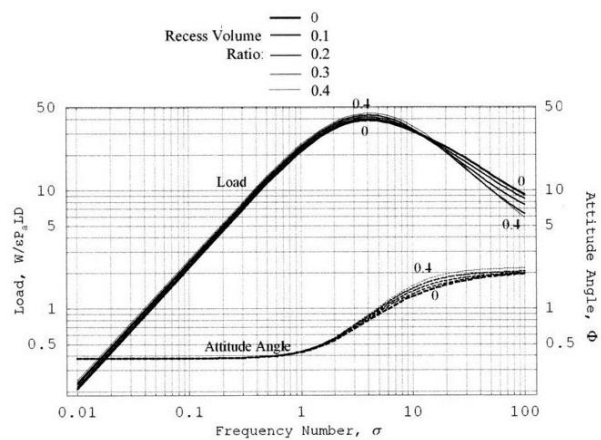


Figure 11. Load, $W/(\epsilon P_a L D)$, and Attitude Angle (ϕ) versus Frequency Number (σ), ($\lambda_i=3$, $P_s=2$, $L/D=1$)

Figure 11 presents the variation of the dimensionless bearing resultant force and attitude angle versus frequency number σ . The increase in the value of the frequency number increases the value of the attitude angle from 0.5 rad to 1 rad. For the dimensionless bearing total force, it can be noticed that the force presents a maximum for a frequency number of 5.

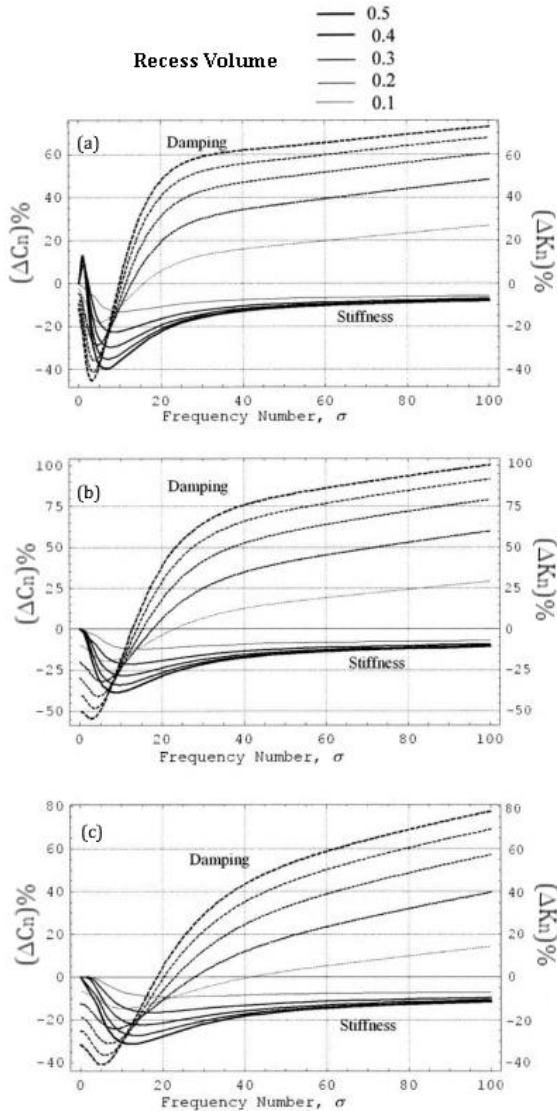


Figure 12. Variation (%) of Normalized EPB Coefficients versus Frequency Number (σ), ($A=0$, $L/D=1$), (a) $\lambda_t=0.1$, (b) $\lambda_t=1$, (c) $\lambda_t=2$

Figure 12 (a), (b), (c) shows the effect of the recess volume on the damping and stiffness coefficients. The dimensionless supply pressure has the value 2 and the dimensionless length is 1. Equations (50) and (51) allow the comparison in % of the stiffness and damping coefficients of an EPB with recess volume against the stiffness and damping coefficients of a similar EPB with 0 recess volume. The percentage variations of the normalized coefficients are plotted against the frequency number, σ . For small values of the frequency number the variation of both the stiffness and damping coefficients presents a local minimum value. Further

increase in the frequency number results in the increase in the damping coefficients over the values calculated for the damping coefficients of the EPB with 0 recess volume. The stiffness coefficients will stabilize at an almost constant value, which is smaller than the values calculated for the stiffness coefficients of an EPB with zero recess volume. This influence of the recess volume on the stiffness and damping coefficients is induced through the coefficient ψ_l defined by equation (23) multiplied by the frequency number σ . The recess volume influence manifests only when is a vibratory movement of the journal.

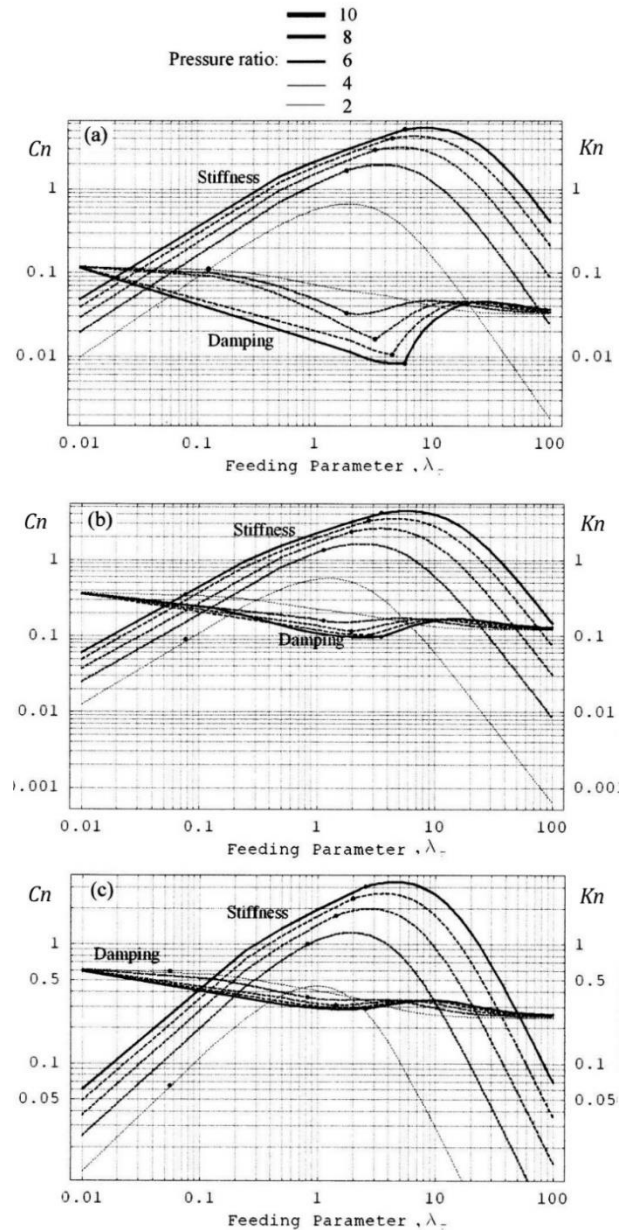


Figure 13. Normalized damping and stiffness versus the feeding parameter λ_t (a) $L/D = 0.5$, (b) $L/D = 1$, (c) $L/D = 1.5$

Figure 13 shows the graph of the normalized bearing coefficients (damping and stiffness) versus the feeding

parameter λ_t . The bearing number (Λ) is zero, therefore the normalized damping and stiffness coefficients are calculated for static conditions. The transitions from “unchoked flow” to “choked flow” are marked with a circular dot on each plot in the set of figures. It can be seen that the transition occurs for a value of the feeding parameter slightly smaller than the value of the feeding parameter associated with the maximum stiffness (and local minimum damping). This pattern possible explanation may be that for “choked flow”, the dimensionless mass flow (m_0) through the bearing remains constant at all times regardless, of the increase of the supply pressure. Therefore, the radial force and respectively the normalized stiffness coefficient, which are dependent on the supply pressure, will achieve maximum values around this transition point. The graphs show that higher values of the supply pressure have the effect of increasing the normalized stiffness. The effect of higher values of the supply pressure on the normalized damping coefficient is negligible because it is a hydrodynamic effect. For higher values of the dimensionless supply pressure the feeding parameter at which the flow transition occurs is closer to the values of the feeding parameter associated with the local extremes of the normalized damping and stiffness coefficients. The graphs also show that an increase in the dimensionless bearing length results in an increase of the normalized damping coefficient and only in a slight decrease of the normalized stiffness.

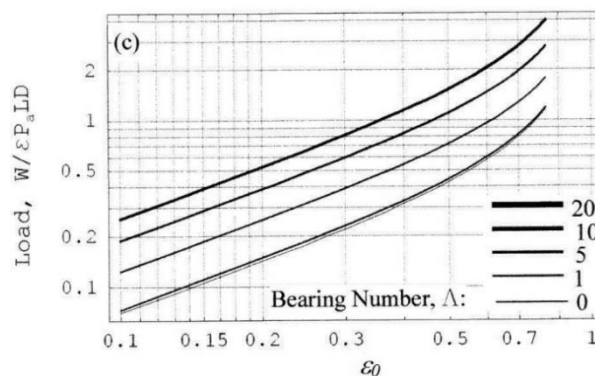
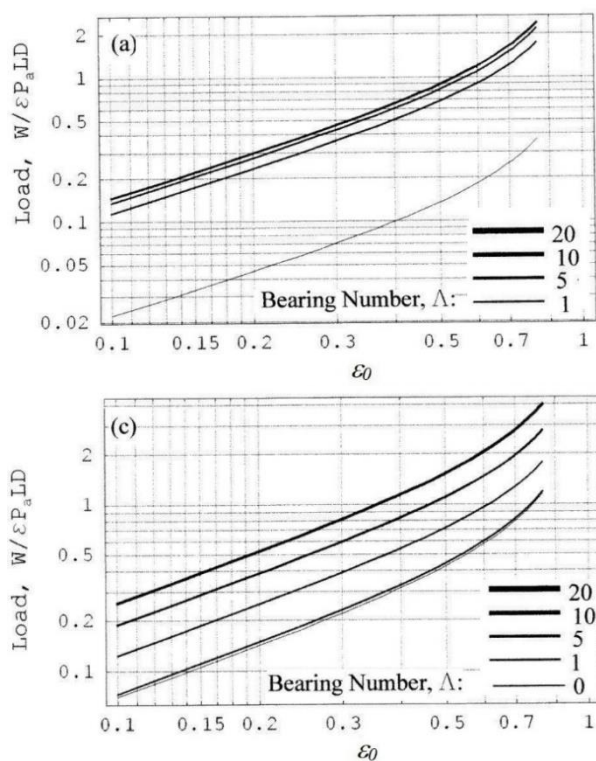


Figure 14. Eccentric Steady State E.P.B. Dimensionless load versus dimensionless eccentricity, ($L/D = 1$), (a) $\lambda_t=0.1$, (b) $\lambda_t=1$, (c) $\lambda_t=5$

Figure 14 (a), (b), (c) shows the variation of the load capacity versus the eccentricity. The dimensionless length has the value 1. In all the cases the increase in the eccentricity results in the increase of the load capacity. An increase in supply pressure has also the effect of increasing the load capacity. The effect of increasing the feeding parameter λ_t on the load capacity is more evident for low values of the eccentricity ratio. For large values of eccentricity ($\epsilon_0 \geq 0.6$) the feeding parameter does not change the values of the absolute force.

5. CONCLUSIONS

This paper presents a novel method which generates the solution of Reynolds boundary value differential equation as a combination of the solutions of two initial value problems (IVP). By using the linearized PH theory, the results for the concentric E.P.B. can be used for solving the steady state eccentric E.P.B.

The method was also used to investigate the influence of the feeding recess volume on the cylindrical whirl threshold ratio and bearing coefficients as well as for the calculation of the transition point between unchoked to choked flow. The results have engineering significance as the EPB coefficients are shown to vary considerably due to the interaction between the recess volumes and the journal vibration. Also, the transition from choked to unchoked flow changes the gas bearing dimensionless flow and, as a result, the inlet pressure values.

The Mathematica program used to implement the proposed method has the advantage that it does not require grid spacing or an estimated number of intermediate points. It employs standard Mathematica build-in symbols, therefore easier to design and use for engineering applications. The calculated results and graphs are in fair agreement with available foundational experimental and theoretical published work. With further modifications the proposed method may be

suitable for the analysis of the whirl and hammer effect
instability of a loaded, eccentric E.P.B.

Grateful acknowledgement to Dr. R. Gohar (Imperial
College of Science, Technology and Medicine, London,
UK) for his detailed manuscript review and pertinent
suggested corrections.

References:

- Ascher, U., & Russell R.D. (1981). Reformulation of Boundary Value Problems into "Standard" Form. *SIAM Review*, 23(2), 238-254. doi.org/10.1137/1023039
- Ausman, J. S. (1961). An Improved Analytical Solution for Self-Acting Gas Journal Bearings Of Finite Length, *Journal of Basic Engineering, Trans. ASME, Series D*, 83(2), 88-92. doi.org/10.1115/1.3658920
- Cazan, A., Gohar R. & Safa M. M. (2002). Externally pressurized gas bearings in a mixed configuration, *Proceedings of the Institution of Mechanical Engineers, Part K: Journal of Multi-body Dynamics*, 216(2), 181-189. doi.org/10.1243/14644190260070411
- Fleming, D. P. (1970). *Zero Load Stability of Rotating Externally Gas-Lubricated Journal Bearings*, *Journal of Lubrication Technology*, 92(2), 325-334. doi.org/10.1115/1.3451403
- Ghosh M. K., Majumdar, B. C. J., & Sarangi, M. (2014). *Fundamentals of fluid Film Lubrication*. McGraw Hill Education, pp. 534-536.
- Klamkin, M. S. (1970). Transformation of Boundary Value Problems into Initial Value Problems. *Journal of Mathematical Analysis and Applications*, 32(2), 308-315. doi.org/10.1016/0022-247X(70)90299-4
- Liu, Z. S., Zhang, G. H., & Xu, H. J. (2008) Performance analysis of rotating externally pressurized air bearings, *Proceedings of the Institution of Mechanical Engineers, Part J: Journal of Engineering Tribology*, 223(4), 653-663, doi.org/10.1243/13506501JET510
- Lund, J., W. (1967). A Theoretical Analysis of Whirl Instability and Pneumatic Hammer for a Rigid Rotor. In Pressurized Gas Journal Bearing, *Journal of Lubrication Technology, Trans ASME, Series F*, 89(2), 154-165. doi.org/10.1115/1.3616933
- Lund, J., W. (June 1964). The Hydrostatic Gas Journal Bearing with Journal Rotation and Vibration, *Journal of Basic Engineering, Trans. ASME, Series D*, 86(2), 328-336. doi.org/10.1115/1.3653073
- Mori, A., & Mori, H., (1973). An application of pneumatic phase shifting to stabilization of externally pressurized journal gas bearings, *J. Lubr. Technol.*, 92(1), 33-41. doi.org/10.1115/1.3451732
- Mori, H., & Mori, A. (1971). A stabilizing method of the externally pressurized gas journal bearings. *6th Int. Gas Bearing Symp.*, Southampton, pp. 4.
- Pink, E. G. (1981). Characteristics of orifice compensated hybrid journal bearings". *8th Gas Bearing Symposium*, 3, 29-44.
- Pink, E. G. (1976). An experimental investigation of externally pressurized gas journal bearings and comparison with design method predictions. *7th Gas Bearing Symposium*, Churchill College, Cambridge, England, pp. G3, 41-59.
- Powell, J. W. (1963). Gas behavior and load capacity of hydrodynamic gas journal bearings. *The Institute of Mechanical Engineers, proceedings of the conference on lubrication and wear*.
- Uneeb, M. & Gohar, R. (1997). Sleeve Dampers for externally pressurized Gas Journal Bearings. *Lubrication Science* 9(4), 409-434. doi.org/10.1002/lis.3010090406
- Wang, X, Xu, Q., Wang, B., Zhang, L., Yang, H. & Peng, Z. (2017). Numerical Calculation of Rotation Effects on Hybrid Air Journal Bearings. *Tribology Transactions*, 60(2), 195-207. doi.org/10.1080/10402004.2016.1155786
- Zhang H., Zhu C., & Yang Q. (2008) Approximate Numerical Solution of Hydrodynamic Gas Journal Bearings, In: Xiong C., Liu H., Huang Y., & Xiong Y. (eds) *Intelligent Robotics and Applications. ICIRA 2008. Lecture Notes in Computer Science*, 5315, Springer, Berlin, Heidelberg, pp. 260-268,

Adrian Cazan

University of East London,
London,
United Kingdom
adrian.cazan@aurak.ac.ae

Adrian Cazan

American University of Ras Al
Khaimah,
Ras Al Khaimah,
United Arab Emirates
adrian.cazan@aurak.ac.ae
